Nanosphere-in-a-Nanoshell: A Simple Nanomatryushka†

ARTICLE *in* THE JOURNAL OF PHYSICAL CHEMISTRY C · NOVEMBER 2009

Impact Factor: 4.77 · DOI: 10.1021/jp9095387

6 AUTHORS, INCLUDING:

Shaunak Mukherjee
Applied Materials
10 PUBLICATIONS **757** CITATIONS
SEE PROFILE

Naomi J Halas
Rice University
328 PUBLICATIONS **35,534** CITATIONS
SEE PROFILE

Nanosphere-in-a-Nanoshell: A Simple Nanomatryushka†

Rizia Bardhan,[¶,‡,§] Shaunak Mukherjee,[¶,‡,§] Nikolay A. Mirin,[‡,§] Stephen D. Levit,[§] Peter Nordlander,[§,||,⊥] and Naomi J. Halas*[,‡,§,||,⊥,#]

Department of Chemistry, Rice University, Houston, Texas 77005, Laboratory for Nanophotonics, Rice University, Houston, Texas 77005, Department of Electrical and Computer Engineering, Rice University, Houston, Texas 77005, Department of Physics and Astronomy, Rice University, Houston, Texas 77005, Department of Bioengineering, Rice University, Houston, Texas 77005

Received: October 5, 2009; Revised Manuscript Received: October 30, 2009

Spherically concentric nanoparticles, composed of a silica-coated gold nanosphere surrounded by a gold shell layer, possess highly geometrically tunable optical resonances in a compact, sub-100 nm size range. The plasmon modes of this nanostructure, a rudimentary "nanomatryushka", arise from the hybridization of nanosphere plasmons with the bonding and antibonding modes of the surrounding Au shell. Here, Au/SiO_2/Au nanoshells are fabricated in sub-100 nm and sub-150 nm size ranges. Changing the internal geometry of the nanoparticle not only shifts its resonance frequencies, but can also strongly modify the relative magnitudes of the absorption and scattering cross sections, independent of nanoparticle size.

Introduction

Metallodielectric layered nanoparticles and nanostructures form a unique and important class of nanomaterials linked by their ability to manipulate light in similar ways. Their optical properties arise from the surface plasmons supported at their metal-dielectric interfaces. Surface plasmons, whether on closely adjacent nanoparticles[1] or on different metal-dielectric interfaces[2,3] of the same nanoparticle, mix and hybridize in direct analogy with simple quantum systems. These nanostructures form a class of plasmonic "artificial molecules" with hybridized plasmons that are highly dependent on nanoscale geometry.[4] As nanostructures of this type are synthesized with increasingly complex geometries, this paradigm becomes even more important, providing a qualitative understanding of the optical resonances of the nanostructure prior to actual synthesis. The ability to control both near and far field properties from the dipole up has made this family of nanostructures interesting for a broad range of spectroscopic,[5−8] biomedical,[9,10] and photonic applications.[11,12]

Multilayered metallodielectric nanostructures, or "nanomatryushkas", where nanoscale dielectric spacer layers separate concentric metallic layers, are of particular interest. Here, the coupling between the surface plasmons is determined by the thickness of the dielectric spacer layers, which can be controlled in the nanoparticle synthesis.[2,13] A theoretical model of a silver core/shell multilayered nanostructure has shown that large local field enhancements are characteristic of the void between the central metal core and the adjacent, innermost metal shell.[14] Such multilayered shells can act as a collection of optical condensers that focus light toward the center of the structure multiplicatively, resulting in an exponential increase in the near-field enhancements as the number of metal shells increases.[14] This structure is the spherical analog of the plasmonic "snowman", a self-similar chain of adjacent nanoparticles of decreasing size, in which the maximum near field focusing occurs not at the tip of the chain but in the junction between the smallest, terminal nanoparticle and its next-nearest, larger neighbor.[15−17] In addition to these distinctive near-field properties, the far-field properties of concentric nanostructures are also controlled largely by the thickness of the intermediate dielectric layer.[18,19] This geometric "tunability" of the plasmon resonances of the nanoparticle into the near-IR region of the spectrum is highly beneficial for light-based biomedical diagnostics and therapeutics.

Gold nanoshells, consisting of a silica nanoparticle core surrounded by a thin Au shell, have generated significant interest due to their applications in biotechnology and biomedicine. In therapeutic applications, tuning the nanoshell plasmon to the near-IR "water window" of 700−1200 nm allows them to be strong optical absorbers or scatterers in a wavelength region where light penetrates several centimeters into the human body.[20] In this regime, nanoshells can be used as contrast agents for enhancing optical imaging;[21] as photothermal heat sources for cancer therapy[10,22,23] for converting the light they absorb to heat for tumor ablation with near 100% remission rates; and as gene therapy vectors, in which resonant light can release genetic cargo bound to their surfaces.[24] Multiple diagnostic and therapeutic functions can even be designed into the same plasmonic nanoparticle theranostic complex.[25] Although many of these tasks can be achieved with nanoshell complexes in the 150-nm-diameter size range, there are important reasons to develop nanocomplexes that maintain similar optical functionality in smaller size regimes. For the detection and treatment of specific types of tumors, such as brain tumors, nanoparticles in the sub-100 nm size regime are expected to have higher photothermal therapeutic efficacy, since they can surpass the blood-brain barrier (BBB), allowing higher nanoparticle concentrations to accumulate in tumors. The BBB is a physical barrier in the form of tight junctions between epithelial cells which impede the transfer of injected agents in the bloodstream into brain tissue.[26] Development of near-IR resonant plasmonic nanostructures in

† Part of the "Martin Moskovits Festschrift".

* Corresponding author. Phone: (713) 348-5611. Fax: (713) 348-5686. E-mail: halas@rice.edu.
‡ Department of Chemistry.
§ Laboratory for Nanophotonics.
|| Department of Electrical and Computer Engineering.
⊥ Department of Physics and Astronomy.
Department of Bioengineering.
¶ These authors contributed equally to this work.

10.1021/jp9095387
Published on Web 11/19/2009

the sub-100 nm size range will ultimately extend these powerful functionalities to this critical, and largely inaccessible, zone of treatment.

In this study, we demonstrate the fabrication of sub-100 nm and sub-150 nm concentric nanostructures consisting of a solid Au nanoparticle immediately surrounded by a silica dielectric layer and then an outer Au shell. We show that the plasmon resonances of this nanoparticle result from the interaction between the essentially fixed-frequency plasmon response of the central nanosphere with the bonding and antibonding plasmons of the surrounding nanoshell. The coupling of nanosphere and nanoshell plasmons in this nanomatryushka particle provides even greater spectral tunability than for an individual Au nanoshell. We relate the optical spectra of the synthesized nanoparticles directly to the plasmon hybridization model of the nanoparticle. For larger nanomatryushkas of this geometry, we observe an additional quadrupolar mode due to phase retardation.

Experimental Methods

Materials Required. Materials used and their suppliers are as follows: $HAuCl_4 \cdot 3H_2O$ (99%, Sigma), potassium carbonate (K_2CO_3, anhydrous, Fisher), CO gas (Matheson), tetraethyl orthosilicate (TEOS, Sigma), 30% NH_4OH (Fisher), 200 proof ethanol (Decon Laboratories Inc.), *N-n*-butyl-aza-2,2-dimethoxysilacyclopentane (Gelest, SIB1932.4), tetrakis(hydroxymethyl)phosphonium chloride (THPC, Sigma), and 1 M NaOH (Fisher).

Fabrication of Au Nanoparticles. Au nanoparticles were fabricated by reducing Au from a 1% $HAuCl_4-K_2CO_3$ solution with $CO_{(g)}$. Briefly, 25 mg of K_2CO_3 was added to 100 mL of H_2O in an amber glass bottle, and subsequently, 1.5 mL of 1% $HAuCl_4$ was added, and the solution was allowed to age at room temperature, in the dark, for 24−72 h. The 1% $HAuCl_4$ was aged for 14 days prior to adding to the K_2CO_3 solution. The 30-nm-diameter Au nanoparticles were fabricated by aging the 1% $HAuCl_4-K_2CO_3$ solution for 24 h and bubbling $CO_{(g)}$ through the solution for 3 min under vigorous stirring. The 40- and 50-nm-diameter Au nanoparticles were fabricated similarly, except the 1% $HAuCl_4-K_2CO_3$ solution was aged for 48 h. The 80-nm-diameter Au nanoparticles were also synthesized similarly, except the 1% $HAuCl_4-K_2CO_3$ solution was aged for 72 h. The nanoparticles were centrifuged twice, 30 min each time, and redispersed in H_2O. The centrifuge speeds are mentioned in Table 1.

Fabrication of Nanoparticles Coated with Silica. The 80-nm-diameter Au nanoparticles were coated with silica following a procedure similar to that reported previously.[27] Briefly, 7 mL of a concentrated Au nanoparticle solution ($\sim 10^{10}$ particles/mL) was mixed with 40 mL of 200 proof fresh ethanol and 400 μL of 30% NH_4OH, and subsequently, 4 μL of TEOS was quickly added. The reaction was allowed to proceed for 45 min at room temperature under vigorous stirring and then was stored in the refrigerator at 4 °C for 24 h. The following day, the Au/SiO_2 nanoparticles were centrifuged and resuspended in 10 mL of ethanol.

The 30-, 40-, and 50-nm-diameter Au nanoparticles were coated with silica by following a slightly different procedure. Concentrated TEOS and NH_4OH (30%, pH$\sim$12) result in aggregation of the smaller nanoparticles due to charge destabilization at high pH and excess silane coupling agent. Hence, 2 mL of the smaller nanoparticle aqueous solution (5×10^{10} particles/mL) was mixed with 10 mL of 200 proof fresh ethanol and 70 μL of 0.4% NH_4OH (pH $\sim$ 8.5), and subsequently, 50−100 μL of 10 mM ethanolic TEOS solution (11 μL TEOS in 5 mL of ethanol) was quickly added to the reaction mixture. The reaction was allowed to proceed for 45 min at room temperature under vigorous stirring and then was stored in the refrigerator at 4 °C for 24 h. The smaller nanoparticles were not centrifuged but directly used for silane functionalization.

Cyclic Silane Functionalization of Nanoparticles. The smaller Au/SiO_2 nanoparticles (30-, 40-, and 50-nm-diameter) were functionalized with 200−400 μL of 1 mM ethanolic solution of cyclic silane (4 μL of silane to 20 mL of ethanol) for 24 h. The 80-nm-diameter Au/SiO_2 nanoparticles were functionalized with 1 mL of 1 mM ethanolic solution of cyclic silane for 24 h. The silane-functionalized, silica-coated nanoparticles were used directly for the next step without further centrifugation. Excessive centrifugation resulted in aggregation of nanoparticles.

Fabrication of $Au/SiO_2/Au$ Nanoshells. The metal core nanoshells were fabricated by seed-mediated electroless plating of Au onto the silica-coated nanoparticles, as previously reported.[28,29] The precursor particles were prepared by decorating the silica-coated nanoparticles with small gold colloid (2−3 nm) fabricated by the method reported by Duff et al.[30] Briefly, 10 mL of the silane-functionalized, silica-coated nanoparticles was mixed with 40 mL of Duff gold colloid and 2 mL of NaCl (1 M). The precursor particles were left unperturbed for 24 h at room temperature, following which they were centrifuged and redispersed in 5 mL of H_2O. The 1% $HAuCl_4-K_2CO_3$ solution previously prepared was used as the plating solution. A continuous gold shell was grown around the Au/SiO_2 nanoparticles by mixing 3 mL of the plating solution with different aliquots of the precursor particles and bubbling $CO_{(g)}$ for 10 s.[28] The reaction was scaled up to obtain an appropriate volume; centrifuged; and finally, redispersed in H_2O.

Centrifuge Speeds for Nanoparticles of Different Sizes. The following speeds were used:

TABLE 1

diameter	Au nanoparticles	Au/SiO_2 precursor	$Au/SiO_2/Au$ nanoshells
80 nm	1500 rcf	390 rcf	150 rcf
50 nm	1600 rcf	700 rcf	250 rcf
40 nm	1700 rcf	800 rcf	300 rcf
30 nm	1850 rcf	920 rcf	370 rcf

Instrumentation and Modeling. Scanning electron microscope (SEM) images were obtained using a FEI Quanta 400 environmental SEM at an accelerating voltage of 25 kV. Extinction spectra were obtained using a Cary 5000 UV/vis/NIR spectrophotometer. Simulated surface charge plots were performed using the RF module of the commercial Finite Element Method software (COMSOL Multiphysics 3.5a) using three-dimensional scattered harmonic propagation.

Results and Discussion

Plasmon hybridization is a useful tool for interpreting the plasmon modes of complex metallic nanostructures.[2] This approach has been used to explain the resonant modes of a nanomatryushka, in which the plasmon modes of the inner and outer metallic shells hybridize, giving rise to symmetric and antisymmetric plasmon modes.[13] The fabricated $Au/SiO_2/Au$ nanoshell is a simple example of a nanomatryushka, in which the inner solid gold nanosphere can be viewed as a gold nanoshell of zero aspect ratio. The response of this system can

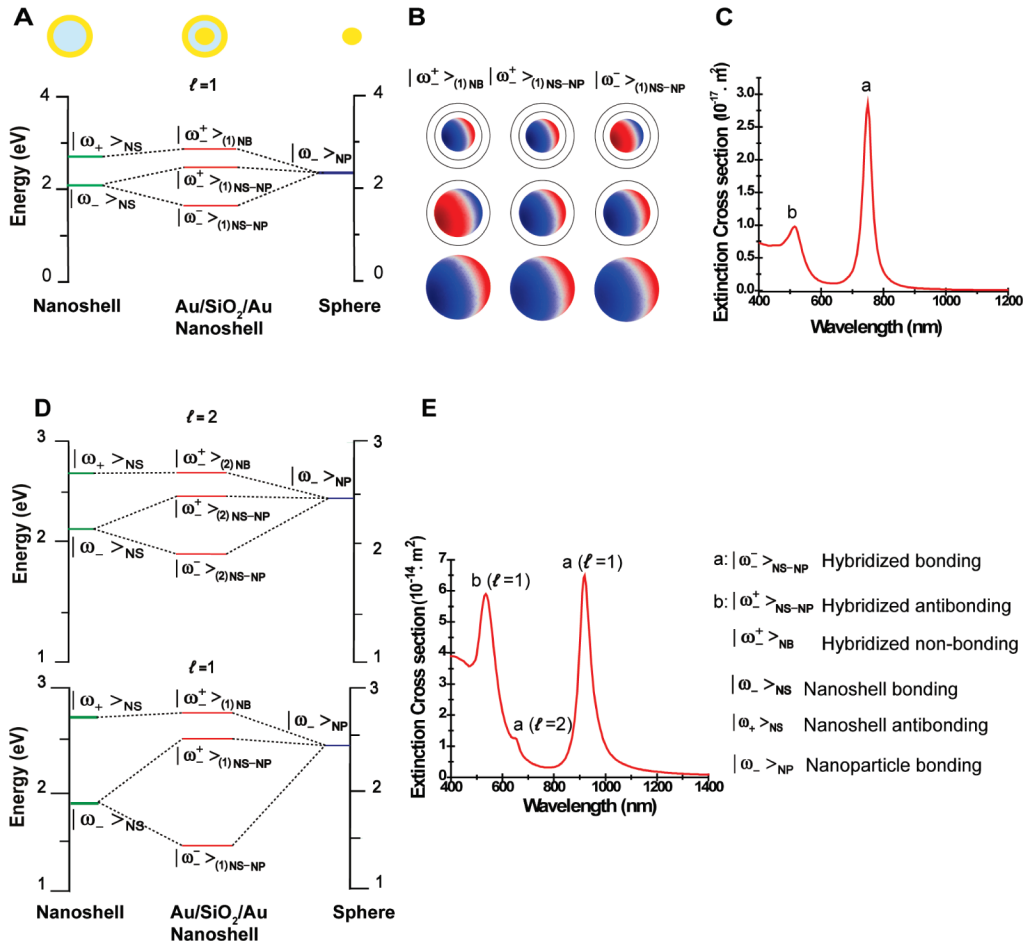

Figure 1. Theoretical analysis of Au/SiO_2/Au nanoshells showing (A) an energy level diagram describing the interaction between the Au nanoparticle and Au nanoshell plasmon resonances resulting in three hybridized energy levels in the quasistatic regime $[r_1, r_2, r_3] = [5, 7, 9]$ nm in $n = 1$ media in the dipole limit. (B) Surface charge distributions on the Au core, inner and outer Au shell interfaces qualitatively corresponding to the three energy eigenmodes. (C) Simulated far-field extinction spectrum of the quasistatic Au/SiO_2/Au nanoshell using the Johnson and Christy dielectric function for gold, with plasmon peaks assigned as (a) hybridized bonding and (b) hybridized antibonding modes. (D) Energy level diagram describing plasmon modes of Au/SiO_2/Au nanoshell having dimensions $[r_1, r_2, r_3] = [40, 55, 65]$ nm showing the hybridized energy level for $l = 1$ dipole (bottom) and $l = 2$ quadrupole (top). (E) Simulated far-field extinction spectrum of this larger Au/SiO_2/Au nanoshell using Johnson and Christy dielectric function for gold with appropriate peak assignments.

be interpreted as the interaction between the primitive plasmon mode of a solid Au sphere and the plasmon modes of the nanoshell.

For a nanomatryushka in the quasistatic regime, $[r_1, r_2, r_3] = [5, 7, 9]$ nm (Figure 1A), where r_1 is the radius of the gold core, r_2 the radius of the silica-coated core, and r_3 the total nanoparticle radius, three dipolar plasmon modes are obtained. Two modes correspond to the hybridization of the low-energy bonding nanoshell plasmon with the nanosphere plasmon, giving rise to a low energy antisymmetric bonding mode ($|\omega_-^-\rangle_{(1)NS-NP}$) and a symmetric antibonding mode ($|\omega_-^+\rangle_{(1)NS-NP}$). Because the interaction between the higher-energy antibonding nanoshell plasmon mode and the nanosphere plasmon is extremely weak, we designate this third mode ($|\omega_-^+\rangle_{(1)NB}$) as a nonbonding mode. This mode is essentially dark, since it has a very small dipole moment due to its appreciable antibonding character.

To determine the nature of the modes that couple to the incident plane wave, finite element method-based simulations were performed for this small quasistatic Au/SiO_2/Au nanoshell. The induced surface charge distribution (Figure 1B) was calculated on the Au core and inner and outer Au shell interfaces. These charge plots fully confirm the hybridization picture. The dipolar bonding $|\omega_-^-\rangle_{(1)NS-NP}$ mode is identified by its distinct regions of positive and negative charge density. The higher-energy, dipolar, antibonding $|\omega_-^+\rangle_{(1)NS-NP}$ mode is recognized by the similar induced charges residing on each of the interfaces, and the higher energy nonbonding mode $|\omega_-^+\rangle_{(1)NB}$ possesses an alternating charge distribution for each successive interface of the nanoparticle.

The calculated far -field extinction spectrum (Figure 1C) shows two distinct plasmon peaks situated at 750 and 515 nm (labeled as "a" and "b"), which corresponds to hybridized bonding $|\omega_-^-\rangle_{(1)NS-NP}$ and antibonding $|\omega_-^+\rangle_{(1)NS-NP}$ modes. This calculation was performed in vacuum ($\epsilon = 1$) using the experimentally obtained Johnson and Christy dielectric function for gold[31] and a constant dielectric value ($\varepsilon = 2.04$) for silica. The symmetric antibonding mode has a larger dipole moment relative to the antisymmetric bonding mode, which results in a strong coupling to the incident light. However, its overlap with the interband transitions of Au results in significant line width broadening and, therefore, a decrease in the peak amplitude.

The plasmon modes for a larger size Au/SiO_2/Au nanoshell $[r_1, r_2, r_3] = [40, 55, 65]$ nm were calculated in the same manner, and the modes are identified using the plasmon hybridization model. (Figure 1D). As for the small quasistatic shell in Figure 1A−C, the same three dipolar hybridized modes are formed. The simulated far-field extinction spectrum of this larger Au/SiO_2/Au nanoshell exhibits three peaks, positioned at 920, 650,

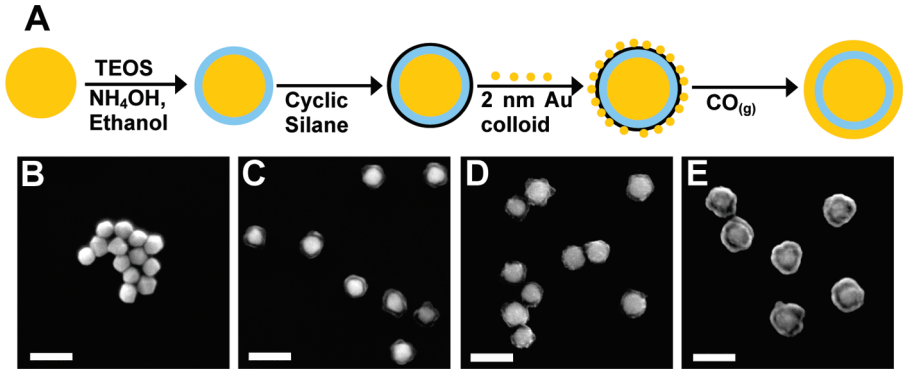

Figure 2. (A) Schematic representation of the fabrication procedure of Au/SiO_2/Au nanoshells. SEM images showing (B) Au nanoparticles of radius, $r_1 = 40 \pm 4$ nm, (C) Au nanoparticles coated with 15 ± 2 nm SiO_2 epilayer, (D) Au/SiO_2 nanoparticles decorated with 2 nm Au colloid, (E) Au/SiO_2/Au nanoshells with dimensions $[r_1, r_2, r_3] = [40, 55, 65]$ nm. The scale bar is 200 nm.

and 535 nm (labeled as a ($l = 1$), a ($l = 2$), and b ($l = 1$) in Figure 1E). The peak at 920 nm is the dipolar bonding mode ($|\omega_-^-\rangle_{(1)NS-NP}$), and the peak at 535 nm is the dipolar antibonding mode ($|\omega_-^+\rangle_{(1)NS-NP}$). The relative intensity of the antibonding mode is higher than for the small quasistatic nanoshell because here, it is shifted further away from the interband transition threshold. The additional mode that appears as a weak shoulder at 650 nm is a quadrupolar bonding mode ($|\omega_-^-\rangle_{(2)NS-NP}$), which can be excited because of phase retardation.

The Au/SiO_2/Au nanoshells were experimentally fabricated, as shown schematically in Figure 2. The synthesis technique developed here is originally adapted and modified from one reported previously.[32] Au nanoparticles of various sizes are initially coated with an epilayer of amorphous SiO_2 by the condensation of tetraethyl orthosilicate in an alkaline medium. Typically, NH_4OH (pH 8−12) is used to initiate this base-catalyzed reaction. The Au/SiO_2 nanoparticles were then functionalized with a cyclic silane (*N*-*n*-butyl-aza-2,2-dimethoxysilacyclopentane). The use of cyclic azasilanes has several advantages compared to the use of alkyl trialkoxy silane coupling agents, such as 3-aminopropyltriethoxysilane (APTES) and 3-mercaptopropyltriethoxysilane (MPTES). Alkyl trialkoxy silanes undergo stepwise hydrolysis in alkaline aqueous media to form the corresponding silanol and subsequent condensation to siloxanes.[33] The hydrolysis is relatively faster than the condensation reaction. During the condensation reaction, depending on the amount of water present, polymerization of the silanes may occur,[33] which often results in nanoparticle agglomeration.

Cyclic azasilanes, alternatively, are particularly useful in surface modification of hydroxyl-containing nanoparticles, since they cause significantly less nanoparticle flocculation. Under basic conditions, cyclic azasilanes undergo ring-opening by hydrolytic cleavage of the C−N bond which has a lower bond energy (320 kJ mol^{-1}) than the Si−O bond (450 kJ mol^{-1}).[34] Due to this ring-opening mechanism, cyclic azasilanes relieve the ring strain and, consequently, hydrolyze faster. Therefore, unlike APTES and MPTES, cyclic azasilanes do not require water as a catalyst for hydrolysis, resulting in no reaction byproducts. Therefore self-polymerization of the silane is substantially reduced, resulting in less nanoparticle aggregation.[34] Subsequent to silanization, small Au colloids (2−3 nm diameter) were attached to the silane-functionalized Au/SiO_2 nanoparticles, which serve as nucleation sites for the electroless plating of the outer Au shell layer onto the nanoparticle surface. A complete outer Au layer is formed by reducing Au from a 1% $HAuCl_4$ aqueous solution in the presence of gaseous CO as the reducing agent.[28,29] This synthesis technique allows the fabrication of relatively monodisperse nanostructures with a complete and homogeneous outer Au layer. Scanning electron microscope images of the nanostructures at various stages of the fabrication procedure are shown in Figure 2B−E. Au nanoparticles of radius 40 ± 4 nm (Figure 2B) coated with a 15 ± 2 nm layer of silica (Figure 2C) were functionalized with silane and decorated with 2−3-nm-diameter Au colloid (Figure 2D). Completed Au/SiO_2/Au nanoshells with dimensions $[r_1, r_2, r_3] = [40, 55, 65]$ nm are shown in Figure 2E.

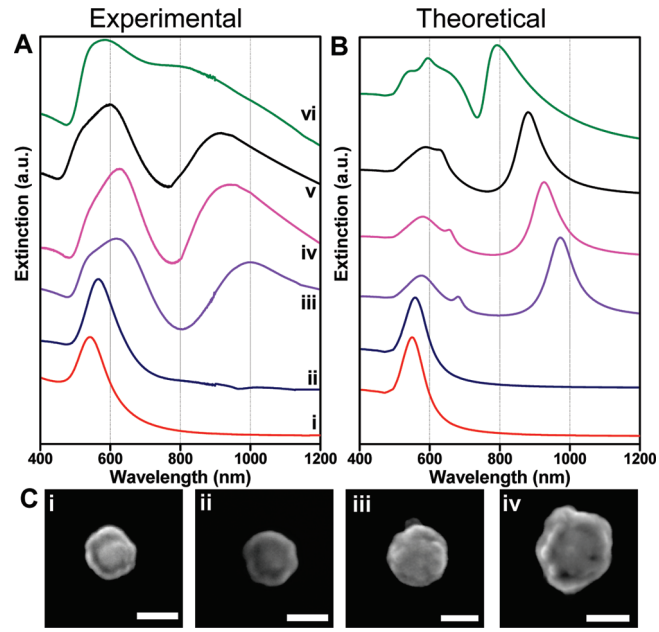

Figure 3. (A) Experimental extinction spectra of (i) Au nanoparticles of radius $r_1 = 40$ nm, (ii) Au/SiO_2 nanoparticles, $r_2 = 55$ nm, and Au/SiO_2/Au nanoshells where (iii) $r_3 = 65$ nm, (iv) $r_3 = 68$ nm, (v) $r_3 = 73$ nm, and (vi) $r_3 = 86$ nm. (B) Theoretical spectra corresponding to the experimental spectra from part A. The spectra are color -coordinated and offset for clarity. (C) SEM images of Au/SiO_2/Au nanoshells corresponding to the spectra from part A. (i) $r_3 = 65$ nm, (ii) $r_3 = 68$ nm, (iii) $r_3 = 73$ nm, and (iv) $r_3 = 86$ nm. The scale bar is 100 nm.

The experimentally observed plasmon resonances of the Au/SiO_2/Au nanoshell solutions of varying dimensions, dispersed in aqueous media, are shown in Figure 3A. The extinction spectra of the core Au nanoparticles of radius ~40 nm and the Au/SiO_2 nanoparticles of radius ~55 nm are shown in Figure 3A,i−ii. For these nanoparticles, the plasmon resonance of the core nanosphere redshifts from 550 (in aqueous solution) to 562 nm after coating with SiO_2 due to the higher refractive index of SiO_2 ($n = 2.04$), as compared to H_2O ($n = 1.33$). Extinction

spectra of Au/SiO_2/Au nanoshells with the same inner nanosphere radius and spacer layer but with increasing thickness of the outer core are shown in Figure 3A,iii−vi. The observed optical spectra of these structures are dramatically different from those of the Au/SiO_2 nanoparticles. A new dipolar bonding resonance is observed in the NIR, which blueshifts across the 1000−800 nm wavelength range with increasing shell thickness. Specifically, as the outer Au shell thickness increases from 10 to 13, 18, and 31 nm, the dipolar bonding resonance blueshifts from 990 nm to 930, 885, and 800 nm, respectively. In addition, a new, broad resonance appears at 620 nm when the metallic shell is present (Figure 3A,iii), also shifting to shorter wavelengths with increasing shell thickness (Figure 3A,iv−vi).

The theoretical extinction spectra corresponding to the Au/SiO_2/Au nanoshells are shown in Figure 3B. The calculated optical spectra were obtained using Mie theory, assuming a symmetric nanostructure with a spherical Au core, and a spherically symmetric SiO_2 layer and outer Au shell. Johnson and Christy gold permittivity[31] was used in these calculations. The maxima in each calculated extinction spectrum correspond well to those observed in the experimental spectra. The blueshifting resonances are the hybridized dipole bonding, $|\omega_-^-\rangle_{(1)NS-NP}$, and dipole antibonding, $|\omega_-^+\rangle_{(1)NS-NP}$ modes of the Au/SiO_2/Au nanoshells, (Figure 1D). For increasing shell thickness, the interaction between the cavity and sphere plasmons in the nanoshell decreases, resulting in a blue shift of the bonding nanoshell plasmon resonance (Figure 3B). The smaller narrow resonant feature observed in the theoretical spectra, which blue-shifts from 685 to 600 nm as the outer Au shell thickness increases is the quadrupole bonding mode, ($|\omega_-^-\rangle_{(2)NS-NP}$) indicated in Figure 1E. Experimentally, this spectral feature is observed as a line shape modulation and, in fact, appears both broader and stronger in the experimental spectra than in the theoretical calculations. The broad line width of this feature is due to the inhomogeneous broadening characteristic of the optical spectroscopy of nanoparticle ensembles. The fact that this feature is more clearly observable in the experimental spectra than in our calculated spectra we attribute to the reduced symmetry of the nanoparticles themselves; in other words, the irregularities of the synthesized nanoparticles. For structural defects that break the spherical symmetry of the system, such as an outer shell of nonuniform thickness or a nonconcentric alignment of the shells, quadrupole modes will hybridize with dipolar modes, thus strongly enhancing their brightness.[35] SEM images of the Au/SiO_2/Au nanoshells corresponding to the experimentally observed optical spectra are shown in Figure 3C,i−iv, in the order of increasing Au shell thickness.

The optical extinction spectra of several Au/SiO_2/Au nanoshells in the sub-100 nm diameter regime and their corresponding SEM images are shown in Figure 4. The optical spectra shown in Figure 4A,i−ii represent Au/SiO_2/Au nanoshells equivalent in overall dimensions, but as the size of the Au core increases from $r_1 = 15$ to 20 nm, the intermediate SiO_2 layer thickness is decreased. This results in a redshift of the $|\omega_-^-\rangle_{(1)NS-NP}$ plasmon resonance from 660 to 730 nm due to an increase in the interaction between the plasmons supported by the Au nanosphere core and the Au outer shell layer. The spectra in Figure 4A,iii−iv show redshifts of the $|\omega_-^-\rangle_{(1)NS-NP}$ mode from 755 to 790 nm as the outer Au layer thickness decreases while all other dimensions remain constant. Theoretical Mie extinction spectra of the sub-100 nm Au/SiO_2/Au nanoshells are shown in Figure 4B and quantitatively reproduce the experimental data in Figure 4A. SEM images of Au nanoparticles of radius 25 ± 3 nm and

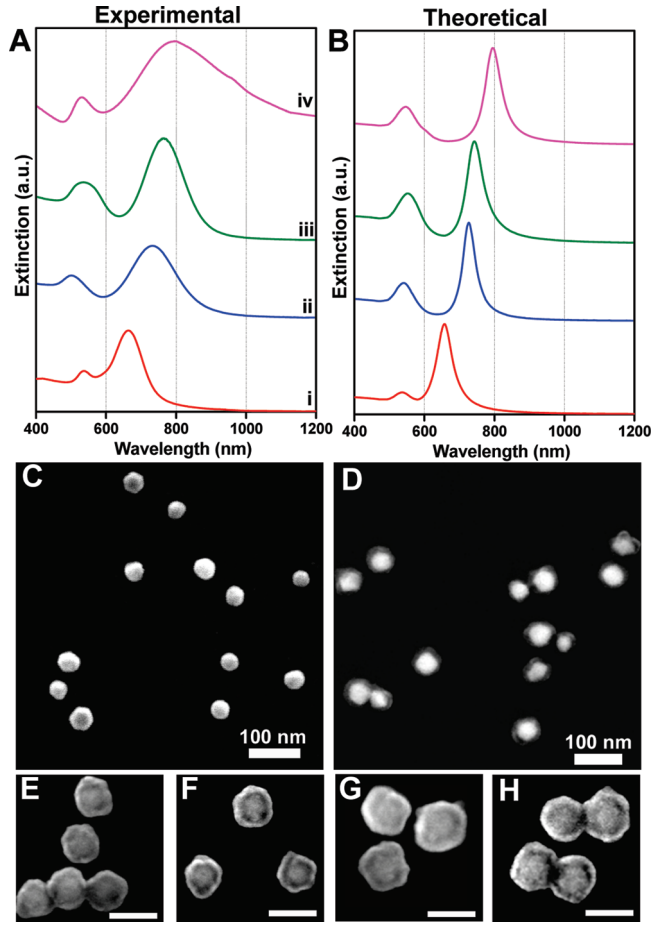

Figure 4. (A) Experimental extinction spectra of sub-100 nm Au/SiO_2/Au nanoshells with different dimensions: (i) [r_1, r_2, r_3] = [15, 30, 42] nm, (ii) [r_1, r_2, r_3] = [20, 30, 42] nm, (iii) [r_1, r_2, r_3] = [25, 37, 51] nm, and (iv) [r_1, r_2, r_3] = [25, 37, 47] nm. (B) Theoretical spectra corresponding to the experimental spectra in part A. The spectra are color-coordinated and offset for clarity. SEM images of (C) Au nanoparticles of radius $r_1 = 25 \pm 3$ nm and (D) coated with a 12 ± 2 nm SiO_2 epilayer. Sub-100 nm Au/SiO_2/Au nanoshells corresponding to the spectra from part A. (E) [r_1, r_2, r_3] = [15, 30, 42] nm. (F) [r_1, r_2, r_3] = [20, 30, 42] nm. (G) [r_1, r_2, r_3] = [25, 37, 51] nm. (H) [r_1, r_2, r_3] = [25, 37, 47] nm. The scale bar is 100 nm.

those coated with a homogeneous 12 ± 2 nm layer of SiO_2 are shown (Figure 4C, D). The SEM images of the sub-100 nm Au/SiO_2/Au nanoshells corresponding to the experimental extinction spectra are also shown (Figure 4E−H). The inner Au core is clearly visible when the silica layer thickness and outer Au shell layer are on the order of ∼10 nm.

Upon illumination with resonant light, metallic nanoparticles will preferentially scatter or absorb light or some combination of the two.[36] In applications, scattering is useful for contrast enhancement in bioimaging. Absorption and its subsequent photothermal heating, which occurs due to nonradiative plasmon decay, results in the therapeutic actuation of hyperthermic cell death or oligonucleotide release. For simple nanoparticles, the absorption and scattering efficiencies are mainly a function of nanoparticle size; for layered nanoparticles, this relationship becomes more complex and geometry-dependent. For multilayered nanomatryushkas, their relative absorption and scattering efficiencies can be modified for a fixed nanoparticle size by varying the internal geometry. The calculated absorption and scattering profiles of the sub-100 nm Au/SiO_2/Au nanoshells fabricated here are shown in Figure 5. For fixed nanoparticle size, an increase in the radius of the Au core and a decrease in

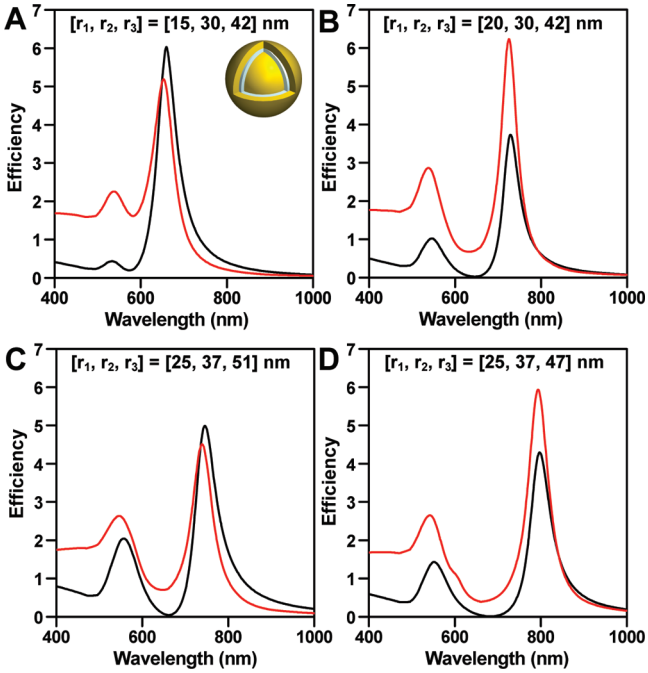

Figure 5. Calculated absorption (red) and scattering (black) efficiencies of Au/SiO_2/Au nanoshells of different sizes: (A) [r_1, r_2, r_3] = [15, 30, 42] nm, (B) [r_1, r_2, r_3] = [20, 30, 42] nm, (C) [r_1, r_2, r_3] = [25, 37, 51] nm, and (D) [r_1, r_2, r_3] = [25, 37, 47] nm.

the silica layer increase the coupling between the core and shell plasmons and results in an increase in absorption efficiency. As seen here, this dependence can be quite significant: by increasing core radius and reducing silica spacer layer thickness each by only 5 nm, the relative absorption efficiency increases from 46% to 63% for the same overall size nanoparticle (Figure 5A, B). This suggests that for bioimaging applications, in which a larger scattering cross section is preferable, Au/SiO_2/Au nanoshells with a thicker intermediate silica layer (>10 nm) would be more efficient, whereas for therapeutic-actuation applications, in which a larger absorption cross section is desired, a geometry with thinner silica layers (≤10 nm) would be preferred. The relative absorption and scattering efficiencies can also be modified by altering the outer Au shell thickness. A nanomatrushka with a thicker Au shell (>10 nm) has greater scattering efficiency, whereas the thinner Au shell (≤10 nm) has a greater absorption efficiency (Figure 5C-D). Again, the higher absorption efficiency corresponds to the case in which the constituent plasmons of the nanoparticle layers couple most strongly.

Conclusions

The Au/SiO_2/Au nanoshells fabricated in this study are simple examples of nanomatryushkas and provide a high degree of plasmonic tunability. Their small sizes make them extremely versatile and promising for a wide array of optical and biomedical applications. The induced charges at the gold-dielectric interfaces govern both the near-field and far-field properties of the structure. The relative absorption and scattering efficiencies can be controlled by tuning the internal geometry for a fixed outer nanoparticle diameter. The plasmon hybridization model reveals that the spectral modes of this nanoparticle arise due to the coupling between the inner Au core and outer Au shell plasmon modes. Understanding precisely the plasmon response of concentric symmetric nanostructures is fundamentally interesting and may provide routes to a variety of technological applications ranging from novel optical devices to biomedical imaging and the treatment of deadly diseases.

Acknowledgment. We gratefully acknowledge the DoD NSSEFF, the Air Force Office of Scientific Research (F49620-03-C-0068), Robert A. Welch Foundation (C-1220 and C1222), and the Multidisciplinary University Research Initiative (W911NF-04-01-0203) for financial support and SUG@R (Shared University Grid at Rice) team. We thank Lisa Brown and Nicholas King for helpful discussions and Ivan Hernandez for graphic design.

References and Notes

(1) Lassiter, J. B.; Aizpurua, J.; Hernandez, L. I.; Brandl, D. W.; Romero, I.; Lal, S.; Hafner, J. H.; Nordlander, P.; Halas, N. J. *Nano Lett.* **2008**, *8*, 1212.
(2) Prodan, E.; Radloff, C.; Halas, N. J.; Nordlander, P. *Science* **2003**, *302*, 419.
(3) Schierhorn, M.; Liz-Marzán, L. M. *Nano Lett.* **2002**, *2*, 13.
(4) Wang, H.; Brandl, D. W.; Nordlander, P.; Halas, N. J. *Acc. Chem. Res.* **2007**, *40*, 53.
(5) Baik, J. M.; Lee, S. J.; Moskovits, M. *Nano Lett.* **2009**, *9*, 672.
(6) Lee, S. J.; Baik, J. M.; Moskovits, M. *Nano Lett.* **2008**, *8*, 3244.
(7) Levin, C. S.; Kundu, J.; Barhoumi, A.; Halas, N. J. *Analyst* **2009**, *134*, 1745.
(8) Moskovits, M. *Rev. Mod. Phys.* **1985**, *57*, 783.
(9) Larsson, E. M.; Alegret, J.; Käll, M.; Sutherland, D. S. *Nano Lett.* **2007**, *7*, 1256.
(10) Lal, S.; Clare, S. E.; Halas, N. J. *Acc. Chem. Res.* **2008**, *41*, 1842.
(11) Kim, S.; Jung, J.-M.; Choi, D.-G.; Jung, H.-T.; Yang, S.-M. *Langmuir* **2006**, *22*, 7109.
(12) Bardhan, R.; Grady, N. K.; Cole, J. R.; Joshi, A.; Halas, N. J. *ACS Nano* **2009**, *3*, 744.
(13) Radloff, C.; Halas, N. J. *Nano Lett.* **2004**, *4*, 1323.
(14) Xu, H. *Phys. Rev. B* **2005**, *72*, 073405.
(15) Li, K.; Stockman, M. I.; Bergman, D. J. *Phys. Rev. Lett.* **2003**, *91*, 227402.
(16) Bidault, S.; de Abajo, F. J. G.; Polman, A. *J. Am. Chem. Soc.* **2008**, *130*, 2750.
(17) Crozier, K. B.; Togan, E.; Simsek, E.; Yang, T. *Opt. Express* **2007**, *15*, 17482.
(18) Hu, Y.; Fleming, R. C.; Drezek, R. A. *Opt. Express* **2008**, *16*, 19579.
(19) Wu, D. J.; Liu, X. J. *Appl. Phys. B: Laser Opt.* **2009**, *97*, 193.
(20) Weissleder, R. *Nat. Biotechnol.* **2001**, *19*, 316.
(21) Gobin, A. M.; Lee, M. H.; Halas, N. J.; James, W. D.; Drezek, R. A.; West, J. L. *Nano Lett.* **2007**, *7*, 1929.
(22) Choi, M.-R.; Stanton-Maxey, K. J.; Stanley, J. K.; Levin, C. S.; Bardhan, R.; Akin, D.; Badve, S.; Sturgis, J.; Robinson, J. P.; Bashir, R.; Halas, N. J.; Clare, S. E. *Nano Lett.* **2007**, *7*, 3759.
(23) Hirsch, L. R.; Stafford, R. J.; Bankson, J. A.; Sershen, S. R.; Rivera, B.; Price, R. E.; Hazle, J. D.; Halas, N. J.; West, J. L. *Proc. Natl. Acad. Sci. U.S.A.* **2003**, *100*, 13549.
(24) Barhoumi, A.; Huschka, R.; Bardhan, R.; Knight, M. W.; Halas, N. J. *Chem. Phys. Lett.* **2009**, *482*, 171−179.
(25) Bardhan, R.; Chen, W.; Perez-Torres, C.; Bartels, M.; Huschka, R. M.; Zhao, L. L.; Morosan, E.; Pautler, R.; Joshi, A.; Halas, N. J. *Adv. Func. Mater.* **2009**, in press (DOI: 10.1002/adfm.200901235).
(26) Ferrari, M. *Nature Rev. Cancer* **2005**, *5*, 161.
(27) Bardhan, R.; Grady, N. K.; Halas, N. J. *Small* **2008**, *4*, 1716.
(28) Brinson, B. E.; Lassiter, J. B.; Levin, C. S.; Bardhan, R.; Mirin, N.; Halas, N. J. *Langmuir* **2008**, *24*, 14166.
(29) Oldenburg, S. J.; Averitt, R. D.; Westcott, S. L.; Halas, N. J. *Chem. Phys. Lett.* **1998**, *288*, 243.
(30) Duff, D. G.; Baiker, A.; Edwards, P. P. *Langmuir* **1993**, *9*, 2301.
(31) Johnson, P. B.; Christy, R. W. *Phys. Rev. B* **1972**, *6*, 4370.
(32) Xia, X.; Liu, Y.; Backman, V.; Ameer, G. A. *Nanotechnology* **2006**, *17*, 5435.
(33) Plueddemann, E. P. *Chemistry of Silane Coupling Agents*, 2nd ed.; Plenum Press: New York, 1991; pp 31−53.
(34) Arkles, B.; Pan, Y.; Larson, J.; Berry, D. In *Silanes and Other Coupling Agents*; Mittal, K. L., Ed.; VSP: Boston, 1992, Vol. 3, pp 179−191.
(35) Wang, H.; Wu, Y.; Lassiter, B.; Nehl, C. L.; Hafner, J. H.; Nordlander, P.; Halas, N. J. *Proc. Natl. Acad. Sci. U.S.A.* **2006**, *103*, 10856.
(36) Bohren, C. F.; Huffman, D. R. *Absorption and scattering of light by small particles*; Wiley: New York, 1983.

JP9095387